Supporting Information to
Delayed Exciton Emission and Its Relation to Blinking in CdSe Quantum Dots

Freddy T. Rabouw,[1] Marko Kamp,[2] Relinde J. A. van Dijk-Moes,[1] Daniel R. Gamelin,[3] A. Femius Koenderink,[2] Andries Meijerink,[1] and Daniël Vanmaekelbergh[1,*]

[1] *Condensed Matter and Interfaces, Debye Institute for Nanomaterials Science, Princetonplein 1, 3584 CC Utrecht, The Netherlands*
[2] *Center for Nanophotonics, FOM Institute AMOLF, Science Park 104, 1098 XG Amsterdam, The Netherlands*
[3] *Department of Chemistry, University of Washington, Seattle, Washington 98195–1700, United States*

[*] E-mail: d.vanmaekelbergh@uu.nl

Synthesis of CdSe/CdS/CdZnS/ZnS core–multi-shell QDs following Ref. [1]

Chemicals used. $Cd(Ac)_2$ (Sigma-Aldrich, 99%), diethylzinc (Et_2Zn, Sigma Aldrich, 1.0 M solution in hexane), oleic acid (OA, Sigma-Aldrich, 90%), octadecene (ODE, Sigma-Aldrich, 90%), octadecyl amine (ODA, Sigma-Aldrich, 90%) selenium (Strem Chemicals, 99.99%), sulphur (Alfa Aesar, 99%), trioctylphosphine (TOP, Sigma-Aldrich, 90%), trioctylphosphine oxide (TOPO, Sigma-Aldrich, 99%), acetone (Merck), hexane (Sigma-Aldrich, anhydrous, 99.8%), methanol (Sigma-Aldrich, anhydrous, 99.8%), butanol (Sigma-Aldrich, anhydrous, 99.8%), toluene (Sigma-Aldrich, anhydrous, 99.8%).

Precursor preparation. Cadmium precursor I [0.1 M $Cd(OA)_2$] was prepared by mixing OA (3.68 g), ODE (25.92 g) and $Cd(Ac)_2$ (0.64 g), and heating to 150°C under vacuum for 2 h. Cadmium precursor II [0.1 M $Cd(OA)_2$] was prepared by dissolving $Cd(Ac)_2$ (1.10 g) in OA (10.83 g) and ODE (43.20 mL), and heating to 150°C under vacuum for 2 h. Selenium precursor was prepared by dissolving elemental selenium (4.25 g) in TOP (22.5 g) at 50°C, followed by the addition of ODE (35.7 g). Zinc precursor [0.1 M $Zn(OA)_2$] was prepared by dissolving $Zn(Et)_2$ (0.494 g) in OA (5.05 mL) and ODE (19.8 mL) at 310°C. Sulphur precursor solution (0.1 M) was prepared by dissolving sulphur (0.032 g) in ODE (10 mL) at 180°C.

Synthesis of CdSe nanocrystal seeds. CdSe nanocrystal seeds were synthesized in 50 ml three-neck flask using a Schlenk-line. TOPO (1.11 g), ODA (3.20 g) and Se precursor (4.9 g) were mixed, and heated to 295°C. When this temperature was reached, the $Cd(OA)_2$-precursor I (5.2 g) was added rapidly. The mixture was cooled down after 5 min. The particles were diluted by adding 1 equivalent of hexane. The quantum dots were washed by adding 2 equivalents of methanol and collecting the upper hexane layer (coloured) and add 1 equivalent of acetone to precipitate the QDs. Finally, the nanocrystal seeds were dissolved in toluene.

Growth of a CdS/CdZnS/ZnS shell. The Cd-, Zn-, and Cd/Zn-precursor solutions were kept at about 80°C, the sulphur precursor solution at room temperature. The CdSe seeds (10^{-7} M of QDs with 3.4 nm diameter in toluene), ODE (5.0 g) and ODA (1.5 g) were mixed and heated to 150°C for 1 h to remove all toluene. The reaction temperature was then increased to 240°C. The shell was grown layer-by-layer under N_2 by injecting a precursor solution every 30 min, alternating cation and anion precursors. 6 layers of CdS, 1 layer of CdZnS, and 1 layer of ZnS were grown. After the final injection of sulphur precursor the reaction was kept at 240°C for 1 h. It was then allowed to cool down to room temperature and diluted with 1 equivalent of toluene. The particles were washed by precipitation using 2 equivalents of a butanol:methanol (1:2) mixture, and centrifugation. The final product was dissolved in toluene.

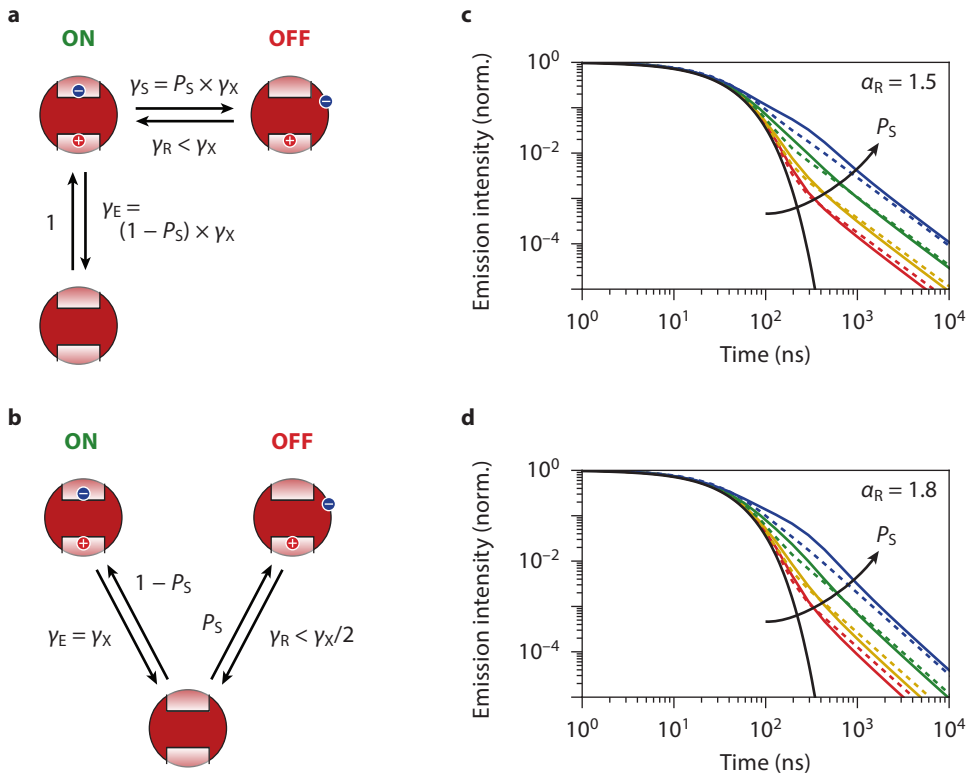

Figure S1 — Photoluminescence decay following charge carrier trapping, storage and release.

Power-law decay contains an infinite number of exponents. To get a power-law decay of the delayed emission $I(t) \propto t^{-\alpha_R}$ at long timescales the exciton recovery rates should be distributed as

$$\rho(\gamma_R) = \begin{cases} \gamma_R^{\alpha_R - 2} & ; \gamma_R < \gamma_{max} \\ 0 & ; \gamma_R > \gamma_{max} \end{cases}, \tag{1}$$

where the upper limit γ_{max} in rates is imposed to avoid a singularity at $t = 0$. This leads to decay dynamics of

$$I(t) = \int_0^{\gamma_{max}} \gamma_R \, \rho(\gamma_R) e^{-\gamma_R t} \, d\gamma_R = [\Gamma(\alpha_R) - \Gamma(\alpha_R, \gamma_{max} t)] \, t^{-\alpha_R}, \tag{2}$$

where the factor between square brackets describes the correction at short times to ensure that the function is well-behaved. To obtain power-law PL decay for the delayed component in our simulation, we make sure that the distribution of release rates of the trapped charge follows Eq. 1. Hence for $\alpha_R < 2$, although very long periods of charge separation are rare, the probability of occurrence per unit of recovery rate is actually higher for slow rates $\gamma_R \approx 0$ than for fast rates $\gamma_R \approx \gamma_{max}$.
The difficulty now lies in the choice for γ_{max}. In principle, there is no reason to assume that the recovery rates are widely (power-law) distributed from s^{-1} to ns^{-1}, but that there is some finite upper limit. However, we can make use of the fact that if at a certain point in time a trap is active with a recovery rate of order ns^{-1} or faster, it will hardly affect the dynamics of photon emission. More precisely, in that case the rate limiting step is the emission process itself, not detrapping and recovery of the delocalised exciton state. The charge-separated state is formed on a timescale of $1/\gamma_X$ (where $\gamma_X = \gamma_E + \gamma_S$ is the total decay rate of the exciton), recovers to the delocalised exciton on a timescale of $1/\gamma_R$, which then emits on a timescale of $1/\gamma_X$. Hence, the shortest possible time scale of delayed emission $2/\gamma_X$.

(a) The kinetic scheme of charge carrier trapping, storage and release. The corresponding three-level rate equation model containing individual rates is

$$\frac{dN_X}{dt} = -\gamma_X N_X(t) + \gamma_R N_S(t) \tag{3}$$

$$\frac{dN_S}{dt} = \gamma_S N_X(t) - \gamma_R N_S(t) \tag{4}$$

$$N_{\mathrm{X}}(0) = 1 \tag{5}$$

$$N_{\mathrm{S}}(0) = 0, \tag{6}$$

where t is the delay time after excitation, N_{X} the population of the exciton state, and N_{S} the population of the charge-separated state. This system of equations can be solved to yield the time evolution of the population in the exciton state $N_{\mathrm{X}}(t)$. In our model the values of γ_{X} and γ_{S} are fixed, while γ_{R} varies on long timescales sampling a power-law distribution. The theoretical PL decay curve $I(t)$ is obtained by integrating over the distribution of recovery rates:

$$I(t) = \gamma_{\mathrm{E}} \langle N_{\mathrm{X}}(t) \rangle = \gamma_{\mathrm{E}} \int_0^{\gamma_{\mathrm{max}}} \rho(\gamma_{\mathrm{R}}) N_{\mathrm{X}}(t)\, \mathrm{d}\gamma_{\mathrm{R}}. \tag{7}$$

We take $\gamma_{\mathrm{max}} = \gamma_{\mathrm{X}}$, *i.e.* we consider only release rates slower than γ_{X}. This choice reflects that only such relatively slow release rates can lead to emission that is clearly delayed compared to normal exciton emission. $N_{\mathrm{X}}(t)$ describes the population decay of the exciton state which is dependent on all rate constants including γ_{R}.

(b) A much simpler model where a fraction $P_{\mathrm{S}} = \gamma_{\mathrm{S}}/\gamma_{\mathrm{X}}$ of the photons are contained in the delayed emission component, with a power-law distributed rate having $\gamma_{\mathrm{max}} = \gamma_{\mathrm{X}}/2$. The factor 1/2 here accounts for the fact that a pathway leading to delayed emission goes through the exciton state with decay rate γ_{X} (at least) twice, as discussed above. The power-law decay of the trapped state is as described by Eq. 2. The rest (fraction $1 - P_{\mathrm{S}}$) of the photons are emitted from the exciton state and contribute an exponential component with decay constant γ_{X}. The total PL decay should follow

$$I(t) = (1 - P_{\mathrm{S}}) \gamma_{\mathrm{X}} \mathrm{e}^{-\gamma_{\mathrm{X}} t} + P_{\mathrm{S}} (\alpha_{\mathrm{R}} - 1) \gamma_{\mathrm{max}}^{1-\alpha_{\mathrm{R}}} \left[\Gamma(\alpha_{\mathrm{R}}) - \Gamma(\alpha_{\mathrm{R}}, \gamma_{\mathrm{max}} t) \right] t^{-\alpha_{\mathrm{R}}} \tag{8}$$

(c,d) The normalized PL decay trace in case of power exponents of **(c)** $\alpha_{\mathrm{R}} = 1.5$ or **(d)** $\alpha_{\mathrm{R}} = 1.8$ for the recovery rates, at different trapping probabilities of $P_{\mathrm{S}} = 0\%$ (black), 5% (red), 10% (yellow), 25% (green), and 50% (blue), and simulated with the three-level rate equation model (solid lines; Fig. S1a, Eq. 7) or with the simpler model (dashed lines; Fig. S1b, Eq. 8). We took $\gamma_{\mathrm{X}} = 1/30$ ns.

Since there is a good correspondence between the two models, we conclude that we can use the analytical expression from the simplified model (Fig. S1b, Eq. 8) to fit the decay dynamics of QD PL under the influence of charge carrier trapping, storage and release. The parameter P_{S} must be interpreted as the probability of charge separation due to charge carrier trapping in a trap with a release rate slower than the intrinsic exciton decay rate ($\gamma_{\mathrm{R}} < \gamma_{\mathrm{X}}$), since only such traps are considered in the rate-equation model (Fig. S1a, Eq. 7).

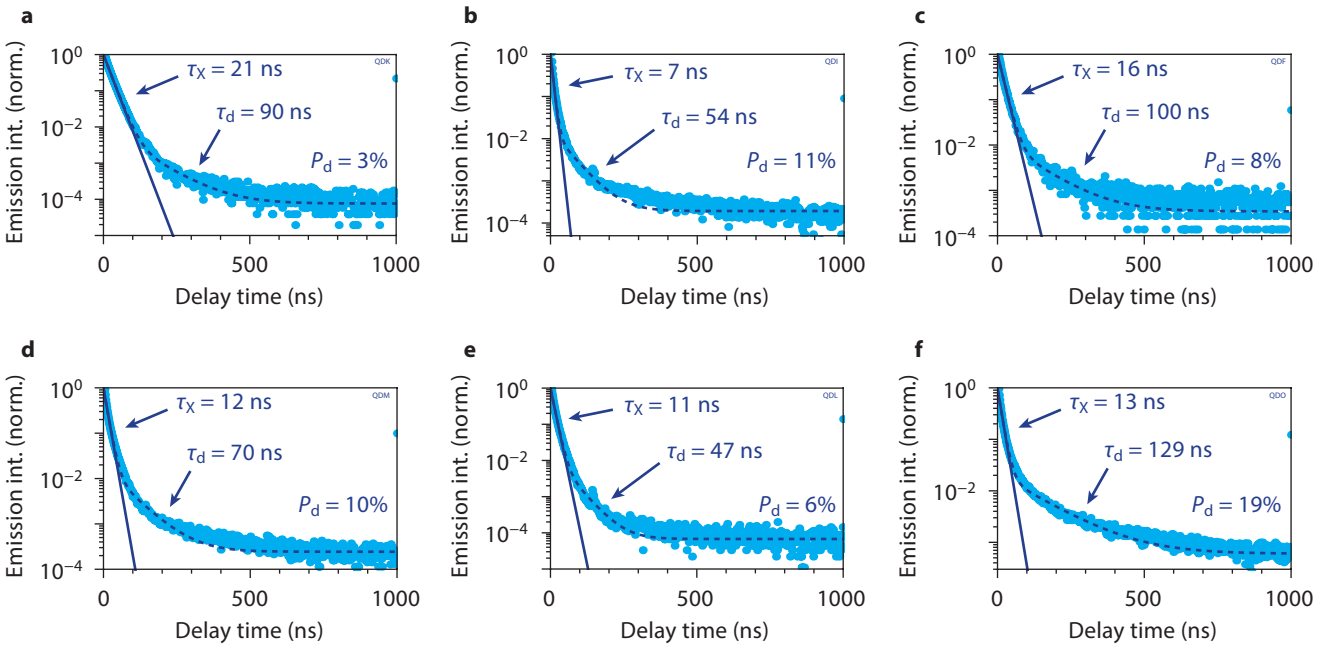

Figure S2 — Delayed emission in the PL decay of single core–shell quantum dots.

(a–f) PL decay curves of six single core–shell QDs. The exciton lifetime τ_X is estimated from a single-exponential fit to the first 100 ns. At longer timescales, typically at a normalised intensity of 10^{-3}–10^{-2}, the decay deviates from this single exponential. A 'delayed component' and a background is added, from which we obtain a 'delayed lifetime' τ_d and the relative contribution of the delayed component $P_d = A_d\tau_d/(A_X\tau_X + A_d\tau_d)$ (where A_X and A_d are the amplitudes of the direct and the delayed component). The fitted values for τ_X, τ_d and P_d are given each panel. The values for P_d are underestimated because part of the delayed contribution is hidden by the background noise with a relative intensity of 10^{-4}–10^{-3}. Indeed, the absolute count rates of the fitted 'background' [which are (**a**) 4, (**b**) 14, (**c**) 3, (**d**) 17, (**e**) 6, and (**f**) 18 counts per time bin of 1.65 ns over a 5 min measurement] show a correlation with with delayed contribution P_d, indicating that the 'background' consists in part of delayed photons. We see that a delayed component is apparent in the PL decay of all single QDs, but the relative contribution varies from QD to QD.

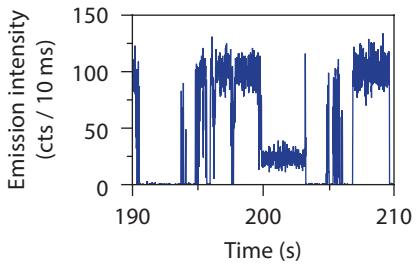

Figure S3 — Discussion of B-type blinking in terms of our new blinking model.

Recently, Galland *et al.* [2] observed what they called 'B-type blinking': the QD blinks between a bright state and state with lower intensity but the same PL decay rate. B-type blinking was ascribed to hot-electron capture, which explains that while traps are active fewer excitations cool down to a ground state exciton (hence the lower intensity) but that the lowest exciton state itself is not affected (hence the unaffected PL decay rate). An alternative explanation of B-type blinking, not involving the scenario of hot-electron capture, would be that in their experiment a type of charge carrier trap is introduced (perhaps in the electrode used) that can make a charge-separated state with a recovery rate γ_{R} on the order of the excitation rate of the QD. If such trap were active, the QD would exhibit ON durations of on average $\langle T_{\mathrm{ON}} \rangle = 1/P_{\mathrm{S}}\gamma_{\mathrm{exc}}$ (with γ_{exc} the excitation rate of the QD) and OFF durations of on average $\langle T_{\mathrm{OFF}} \rangle = 1/\gamma_{\mathrm{R}}$. Averaged over a time bin in the intensity trace, the apparent quantum efficiency the active period of the trap would be $\eta = \langle T_{\mathrm{ON}} \rangle / (\langle T_{\mathrm{ON}} \rangle + \langle T_{\mathrm{OFF}} \rangle) = \gamma_{\mathrm{R}}/(P_S\gamma_{\mathrm{exc}} + \gamma_{\mathrm{R}})$. An apparent quantum efficiency η would correspond to an exciton recovery rate of $\gamma_{\mathrm{R}} = P_S\gamma_{\mathrm{exc}}\eta/(1-\eta)$.

The plot is a zoom-in of the intensity trace of Fig. 3b in the main text, as simulated with our model. It shows a period between 199 s to 203 s where the intensity is at some intermediate level between the brightest state and the darkest state. Note that in our model the OFF state is completely dark, so that intermediate intensities must be due to rapid switching between ON and OFF on timescales faster than the binning time of the intensity trace. The rate of switching is determined by the recovery rate γ_{R}, which can be fixed for a long period T. The intermediate intensity state occurring around $t = 200$ s, with an apparent quantum efficiency of $\eta \approx 25\%$ occurs because during these 4 s the trap has a release rate of $\gamma_{\mathrm{R}} \approx 0.05\ \mu\mathrm{s}^{-1}$.

B-type blinking as observed by Klimovs group occurs between a bright state and a dim state with $6\times$ lower intensity but equal PL lifetime (Figures 4 and 5 in Ref. 2). These measurements were performed with a laser repetition rate of 2.5 MHz, and an excitation fluence resulting in on average 1 absorption event per 5 pulses. (We note that the Methods section is not entirely conclusive on the experimental parameters specific to Figures 4 and 5.) With these experimental parameters, B-type blinking can be explained if the QD or its immediate environment contains a charge-carrier trap with a release rate of $\gamma_{\mathrm{R}} = 10^5\ \mathrm{s}^{-1} \times P_{\mathrm{S}}$. P_{S} is the unknown probability of charge-carrier separation in the QD examined in Ref. 2. For the sake of simplicity, we will assume here that its value is $P_{\mathrm{S}} = 10\%$, in line with our results, corresponding to a release rate of $\gamma_{\mathrm{R}} = 10^4\ \mathrm{s}^{-1}$.

The situation of B-type blinking would be as follows: under the excitation power used, it takes on average 5 laser pulses = 2 μs for the QD to absorb a photon. While in the neutral state, the QD undergoes 'ordinary' optical cycling resulting in direct exciton emission with the ordinary PL lifetime. Charge carrier separation happens on average after 50 laser pulses = 20 μs. Subsequently, the QD remains in the charge-separated state for on average $1/\gamma_{\mathrm{R}} = 100\mu$s, during which it is dark. It then returns to the neutral state, under the emission of a single delayed photon. After that, optical cycling with the ordinary PL lifetime continues. Overall, the QD is emissive for 1/6 of the time resulting in a brightness averaged over a time bin of 50 ms that is $6\times$ lower than the bright state. During the emissive periods (1/6 of the total time), the PL lifetime is the 'ordinary' single-exciton lifetime, because these periods are characterized by ordinary optical cycling in the neutral state.

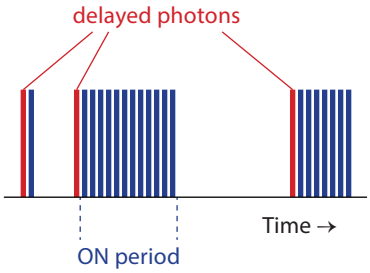

Figure S4 — The delayed contribution in existing blinking models.

We investigate what would be the integrated contribution of delayed emission if we assume, as done in existing blinking models, that ON periods are characterised by uninterrupted optical cycling. We further assume that each laser pulse leads to the absorption of a photon in the QD. The situation would be as in the cartoon. It shows the photon emission from a QD with an exciton lifetime of $\tau = 30$ ns that is excited every time bin of, say, 100 ns. There are ON periods during which each excitation leads to exciton emission (blue bars; uninterrupted optical cycling). Every now and then there is charge carrier separation, after which the QD is dark. At some moment in time the exciton state recovers and emits a delayed photon (red bars). Optical cycling then continues. If the ON periods are power-law distributed (Fig. 1 in the main text, as well as in many other QD samples [3, 4]) and we assume that during ON periods there is only direct exciton emission due to uninterrupted optical cycling, then the contribution of delayed emission can be calculated using the following reasoning.

The contribution of delayed emission is simply the fraction of bars in the diagram that is red. Clearly, every long-lived ON period (say, longer than a ms) would be a huge decrease of the relative number of red bars. The fraction of bars that is red, *i.e.* the contribution of delayed emission, is calculated as

$$P_{\mathrm{d}} = \frac{\int_{t_{\mathrm{min}}}^{t_{\mathrm{max}}} t^{-\alpha}\,\mathrm{d}t}{t_{\mathrm{min}}^{-1}\int_{t_{\mathrm{min}}}^{t_{\mathrm{max}}} t\,t^{-\alpha}\,\mathrm{d}t}. \tag{9}$$

Here the integrations are over all possible durations of ON periods, which range from t_{min} (the repetition period of the laser, which defines the time resolution) to t_{max} (the longest possible ON duration). In the numerator we consider that each possible ON duration contains only a single delayed photon (namely the first; see cartoon). In the denominator we have the total number of photons $t_{\mathrm{min}}^{-1}t$ emitted during an ON period with duration t.

With reasonable values of $t_{\mathrm{min}} = 100$ ns, $t_{\mathrm{max}} = 10$ s, and $\alpha = 1.6$, we get a predicted delayed contribution of $P_{\mathrm{d}} = 4 \times 10^{-4}$. This value is far off from the experimental contribution of approximately 10% (Fig. 3c in the main text, and Supplementary Fig. S2). Clearly, the assumption that ON periods involve uninterrupted optical cycling is inconsistent with our data.

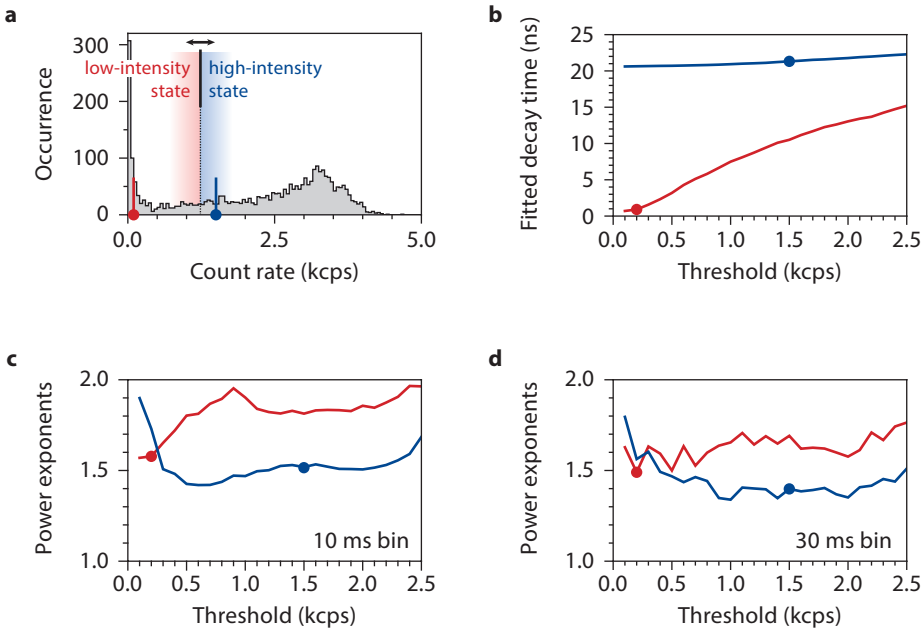

Figure S5 — The choice of threshold in the analysis of the blinking trace.

(a) The intensity histogram of the emission trace of Fig. 1c in the main text, with a binning of 100 ms. For the analysis in the main text, we defined the OFF state as having a count rate less than 0.2 kcps, the ON state as more than 1.5 kcps (indicated with red and blue circles). Here, we investigate the effect of choosing a different threshold on the properties extracted for the highest- and lowest-intensity states. **(b)** The fitted decay time of the low-intensity state (red) and the high-intensity state (blue) as a function of threshold. The dots mark the thresholds chosen in the main text. We see that while the ON-lifetime is more or less independent on the threshold. On the other hand, as soon as high-intensity time bins (>0.2 kcps) are included in the definition of the OFF-state, the fitted OFF-lifetime increases. **(c,d)** The power exponent fitted to the blinking statistics of the low-intensity state (red) and the high-intensity state (blue) as a function of threshold, for a time binning of **(c)** 10 ms or **(d)** 30 ms. As before, the dots mark the thresholds chosen in the main text. We see that, as shown before [5], the exact value for the power exponents depend on the treshold and on the time bin width. However, the power exponents are always around 1.5 for any reasonable choice of parameters (*i.e.* all except a high threshold for the OFF-state).

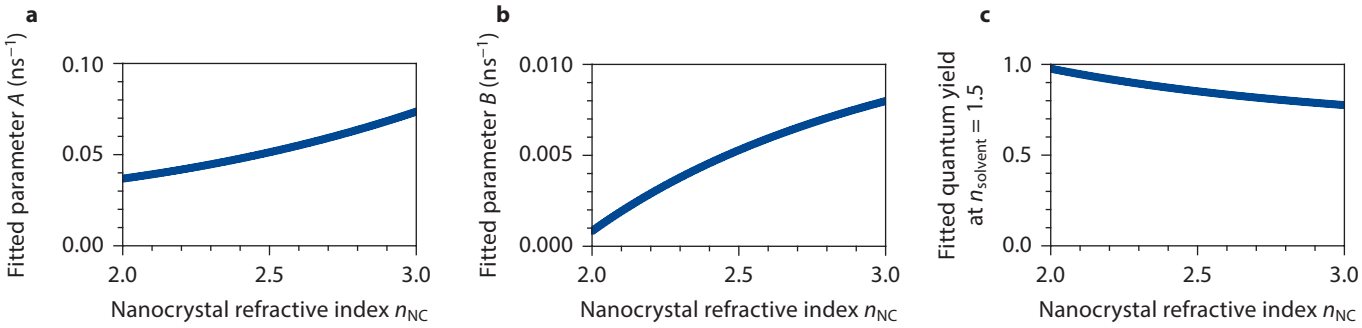

Figure S6 — The nanocrystal refractive index in the nanocrystal-cavity model.

The nanocrystal-cavity model (Eq. 4 in the main text) for the exciton decay rate of a nanocrystal contains three parameters: A parametrizes the strength of radiative decay, B is the nonradiative decay rate, and n_{NC} is the refractive index of the nanocrystal. Note that 'nonradiative' decay of the initial exciton state, may in the end still result in the emission if a photon. If the nonradiative process B is charge carrier separation, the exciton can be restored after s–ms and emit, as we show in this paper.

Because of quantum confinement, semiconductor QDs may have a refractive index different from the bulk material. In our case the strongly quantum-confined states are located in the CdSe core. The 'effective' refractive index of the QDs is however determined mainly by the large volume of CdS shell. We therefore fix this parameter to the CdS bulk value of $n_{\mathrm{NC}} = 2.5$ in the main text. Here we show how the choice for this parameter affects the fit results obtained for **(a)** parameter A, and **(b)** parameter B. The fitted value for A is a factor ~ 3 lower than the theoretical value of $A = 4e^2P^2E/\left(9 \times 4\pi\epsilon_0 m_0^2 c^3 \hbar^2\right) = 0.168$ ns^{-1} estimated for core-only QDs (with P the Kane interband matrix element, and E the energy of the emitted photon) [6]. This difference is in part due to delocalization of charge carriers in the shell of our QDs. Furthermore, we see in **a** and **b** that the choice for a value of n_{NC} can influence the fit result obtained. It also affects the calculated quantum efficiency of the emissive QD (Eq. 5 of the main text; see panel **c**). The calculated quantum efficiency for an environment of $n_{\mathrm{solvent}} = 1.5$ changes from 97% at $n_{\mathrm{NC}} = 2.0$ to 78% at $n_{\mathrm{NC}} = 3.0$. The main conclusion drawn from the nanocrystal cavity model is however robust, namely that the direct decay of emissive QDs in the ensemble is dominated by radiative decay.

[1] Xie, R.; Kolb, U.; Li, J.; Basch, T.; Mews, A. *J. Am. Chem. Soc.* **2005**, *127*, 7480–7488.
[2] Galland, C.; Ghosh, Y.; Steinbrück, A.; Sykora, M.; Hollingsworth, J. A.; Klimov, V. I.; Htoon, H. *Nature* **2011**, *479*, 203–207.
[3] Kuno, M.; Fromm, D. P.; Hamann, H. F.; Gallagher, A.; Nesbitt, D. J. *J. Chem. Phys.* **2001**, *115*, 1028–1040.
[4] Cordones, A. A.; Leone, S. R. *Chem. Soc. Rev.* **2013**, *42*, 3209–3221.
[5] Frantsuzov, P. A.; Volkán-Kacsó, S.; Jankó, B. *Phys. Rev. Lett.* **2009**, *103*, 207402.
[6] Efros, Al. L.; Rosen, M.; Kuno, M.; Nirmal, M.; Norris, D. J.; Bawendi, M. *Phys. Rev. B* **1996**, *54*, 4843–4856.